A Role for DPPX Modulating External TEA Sensitivity of Kv4 Channels

Olaia Colinas, Francisco D. Pérez-Carretero, José R. López-López, and M. Teresa Pérez-García

Departamento de Bioquímica y Biología Molecular y Fisiología e Instituto de Biología y Genética Molecular (IBGM), Universidad de Valladolid y Consejo Superior de Investigaciones Científicas (CSIC), 47003 Valladolid, Spain

Shal-type (Kv4) channels are expressed in a large variety of tissues, where they contribute to transient voltage-dependent K^+ currents. Kv4 are the molecular correlate of the A-type current of neurons (I_{SA}), the fast component of I_{TO} current in the heart, and also of the oxygen-sensitive K^+ current (K_{O2}) in rabbit carotid body (CB) chemoreceptor cells. The enormous degree of variability in the physiological properties of Kv4-mediated currents can be attributable to the complexity of their regulation together with the large number of ancillary subunits and scaffolding proteins that associate with Kv4 proteins to modify their trafficking and their kinetic properties. Among those, KChIPs and DPPX proteins have been demonstrated to be integral components of I_{SA} and I_{TO} currents, as their coexpression with Kv4 subunits recapitulates the kinetics of native currents. Here, we explore the presence and functional contribution of DPPX to K_{O2} currents in rabbit CB chemoreceptor cells by using DPPX functional knockdown with siRNA. Additionally, we investigate if the presence of DPPX endows Kv4 channels with new pharmacological properties, as we have observed anomalous tetraethylammonium (TEA) sensitivity in the native K_{O2} currents. DPPX association with Kv4 channels induced an increased TEA sensitivity both in heterologous expression systems and in CB chemoreceptor cells. Moreover, TEA application to Kv4-DPPX heteromultimers leads to marked kinetic effects that could be explained by an augmented closed-state inactivation. Our data suggest that DPPX proteins are integral components of K_{O2} currents, and that their association with Kv4 subunits modulate the pharmacological profile of the heteromultimers.

The Journal of General Physiology

INTRODUCTION

Voltage-gated K (Kv) channels belonging to the mammalian Kv4 subfamily all rapidly activate and inactivate in response to subthreshold membrane depolarization, giving rise to transient outward K^+ currents that are also characterized by their fast recovery from inactivation (for review see Jerng et al., 2004a). These unique biophysical properties provide a relevant role for Kv4 channels in many excitable tissues. In cardiac cells, Kv4 channels have been shown to represent the molecular correlate of I_{TO} currents, determining the initial phase of action potential repolarization (Barry et al., 1998; Xu et al., 1999). Kv4 channels are also responsible for a large portion of the rapidly inactivating outward K^+ current (A-type current) that controls the shape, frequency, and propagation of action potential in many neurons (Baldwin et al., 1991; Serodio et al., 1994; Johns et al., 1997; Tkatch et al., 2000; Malin and Nerbonne, 2001). As a particular case of neuronal cells, in rabbit carotid body chemoreceptor cells, genes of the Kv4 family have been shown to represent the molecular correlate of the oxygen-sensitive voltage-dependent K^+ current (K_{O2}) originally described in this preparation (Perez-Garcia et al., 2000; Sanchez et al., 2002; López-López et al., 2003).

However, there is a wide variability in gating kinetics, conductance, and pharmacology among these native currents that is partly due to alternative splicing, heteromeric assembly of pore-forming Kvα subunits, RNA editing, and posttranscriptional modifications. This multiplicity is augmented by the interaction of Kv4 channels with their numerous ancillary proteins. Differences in the biophysical properties of the neuronal or cardiac currents and Kv4 channels expressed in heterologous systems have long suggested that the native channel may be a multisubunit complex comprised of Kv4 pore-forming subunits and modulatory proteins (Rudy et al., 1988; Chabala et al., 1993; Serodio et al., 1994). More recently, several reports confirmed that two novel protein families with previously unknown functions, Kv channel interacting proteins (KChIPs) and dipeptidyl aminopeptidase-related proteins (DPPX, DPPY), are critical components of cardiac and neuronal A-type currents that regulate Kv4 trafficking and kinetics (An et al., 2000; Nadal et al., 2003; Jerng et al., 2004b; Jerng et al., 2005; Nerbonne and Kass, 2005; Radicke et al., 2005a; Ren et al., 2005). In fact, in the light of recent findings most ion channels can be envisioned as heteromeric, dynamically assembled multiprotein complexes, to such extent that even though α subunits suffice to form a functional pore, it is not clear whether they actually do

Correspondence to M. Teresa Pérez-García: tperez@ibgm.uva.es

Abbreviations used in this paper: CB, carotid body; HpTx, heteropodatoxin; SEC, siRNA expression cassette; TH, tyrosine hydroxylase.

The Rockefeller University Press $30.00
J. Gen. Physiol. Vol. 131 No. 5 455–471
www.jgp.org/cgi/doi/10.1085/jgp.200709912

so in native tissues. According to this, changes in the level of expression of the different elements of the multimers together with differences in the splice variants present in a tissue could explain the variability in biophysical properties of native currents among different tissues or different cells within the same tissue (Nerbonne, 2000; Jerng et al., 2004a).

This variability does not seem to affect the pharmacological profile of Kv4 currents, which are typically described as 4-AP sensitive and TEA resistant. This holds true when characterizing Kv4 currents in heterologous expression systems (Pak et al., 1991; Jerng and Covarrubias, 1997) and also when studying native currents (Martina et al., 1998; Song et al., 1998), suggesting that the association of Kv4 pore-forming subunits with accessory subunits does not change the pharmacological properties of the heteromultimers. However, in rabbit carotid body (CB) chemoreceptor cells we have observed that transient outward K^+ currents are sensitive to 4-AP (López-López et al., 1993) and heteropodatoxin (HpTx-2) (Sanchez et al., 2002), but can also be blocked by external TEA application. TEA inhibition was observed with TEA concentrations as low as 10 μM, and increases when augmenting TEA up to 10 mM (Kääb et al., 2005). While we have identified Kv3.4 as the highly sensitive TEA component of the transient K^+ current (Sanchez et al., 2002; Kääb et al., 2005), we have no explanation for the blockade of the Kv4 component with low-millimolar TEA concentrations. In the search for an explanation of this perplexing observation, we have explored the possibility that some accessory subunit of Kv4 channels could determine the atypical pharmacological profile of the transient K^+ current in rabbit CB chemoreceptor cells. Among Kv4 auxiliary subunits, the structural properties of DPPX, with a large C-terminal extracellular domain (Wada et al., 1992), made conceivable the hypothesis that its association with Kv4 α subunits could modify the binding of TEA to the external side of the pore. We found that coexpression of DPPX in HEK cells endows Kv4 channels with a new high-affinity binding site for TEA that affects both conductance and kinetic properties of the heteromultimers. Furthermore, we detected high expression levels of DPPX mRNA in rabbit CB chemoreceptor cells (when compared with cerebellar granule neurons), DPPX protein was found to coexpress with Kv4.3, and its functional knockdown with siRNA modified the kinetics of the transient K^+ current and decreased its sensitivity to extracellular TEA, demonstrating the physiological association in a native tissue.

MATERIALS AND METHODS

HEK293 Cell Maintenance and Transfections

HEK293 cells were maintained in DMEM supplemented with 10% FCS (GIBCO BRL), 100 $U \cdot ml^{-1}$ penicillin, 100 $g \cdot ml^{-1}$ streptomycin, and 2 mM L-glutamine. Cells were grown as a monolayer and plated on coverslips (6 mm) placed in the bottom of 35-mm Petri dishes at a density of 2–4 × 10^5 cells/dish the day before transfection. Transient transfections were performed using Lipofectamine 2000 (Invitrogen), with 0.1 μg of plasmid DNA encoding Kv4.1, Kv4.2, or Kv4.3 alone or in combination with 1.5 μg of plasmid DNA encoding DPPX subunit (molar ratio Kv4:DPPX 1:10). In all cases, 0.2 μg of plasmid DNA encoding GFP was included to permit transfection efficiency estimates (20–60%) and to identify cells for voltage-clamp analysis. The plasmids used were rabbit Kv4.3 in pCMV-SPORT (a gift of J.L. Rae, Mayo Clinic, Rochester, MN), rat Kv4.2 in pEGFP-C3 (a gift of D.C. Johns, Johns Hopkins University, St. Louis, MO), mouse Kv4.1 (provided by L. Salkoff, Washington University, St. Louis, MO; and subcloned into pAdTrack), and human DPPX-s in pRc/RSV (obtained from K. Wada, National Institute of Neuroscience, Tokyo, Japan). gWIZ-GFP was purchased from Gene Therapy Systems Inc.

Dissociation and Short-Term Culture of Rabbit Carotid Body Cells

Adult New Zealand rabbits (1.5–2 kg) were anesthetized with intravenous application of sodium pentobarbital (40 mg/kg) through the lateral vein of the ear. After tracheostomy, carotid artery bifurcations were dissected out and animals were killed by intracardiac injection of sodium pentobarbital. All measures were taken to ensure the animals did not suffer distress at any time. The protocols were approved by the Institutional Care and Use Committee of the University of Valladolid and were conducted in accordance with the Guide for the Care and Use of Laboratory Animals (1996. National Academy of Sciences, Washington D.C.). The CBs were enzymatically dispersed as previously described (Pérez-García et al., 1992). Dispersed cells were plated onto poly-L-lysine–coated coverslips with 2 ml of growth medium, and maintained in culture at 37°C in a 5%CO_2 atmosphere up to 96 h.

Electrophysiological Methods

Ionic currents were recorded at room temperature (20–25°C) using the whole-cell or the outside-out configuration of the patch-clamp technique. Whole-cell current recordings and data acquisition from CB chemoreceptor cells were made as previously described (López-López et al., 1997; Sanchez et al., 2002). The coverslips with the attached cells were placed at the bottom of a small recording chamber (0.2 ml) on the stage of an inverted microscope and perfused by gravity with the bath solution. Patch pipettes had resistances ranging from 2 to 4 MΩ when filled with the internal solution. The composition of the bath solution was (in mM) 141 NaCl, 4.7 KCl, 1.2 $MgCl_2$, 1.8 $CaCl_2$, 10 glucose, 10 HEPES (pH 7.4 with NaOH), and the pipette was filled with a solution containing (in mM) 125 KCl, 4 $MgCl_2$, 10 HEPES, 10 EGTA, 5 MgATP (pH 7.2 with KOH).

The currents were recorded using an Axopatch 200 patch-clamp amplifier, filtered at 2 kHz (−3dB, 4-pole Bessel filter), and sampled at 10 kHz. When whole currents were recorded, series resistance was compensated. When leak subtraction was performed, an online P/4 protocol was used. Recordings were digitized with a Digidata 1200 A/D interface, driven by CLAMPEX 8 software (Axon Instruments) in a Pentium clone computer.

Sensitivity of K^+ currents of CB chemoreceptor cells to TEA was analyzed by studying the decrease in the peak current amplitude in depolarizing pulses to +40 mV from a holding potential of −80 mV upon application of increasing concentrations of TEA to the bath solution. Average current amplitude before and after TEA application was used as the control value. Cells in which no washout of the drug could be obtained due to deterioration of seal conditions were discarded for analysis. In the case of transfected HEK cells, and due to the kinetic changes observed upon TEA

application in the presence of DPPX, the magnitude of the block was also determined by calculating the integral of the depolarizing pulses.

Electrophysiological data analyses were performed with the CLAMPFIT subroutine of the PCLAMP software and with ORIGIN 7.5 software (Microcal Inc.). Pooled data are expressed as mean ± SEM. Statistical comparisons between groups of data were performed with the two-tailed Student's *t* test for paired or unpaired data, and values of $P < 0.05$ were considered statistically different.

siRNA Design and Construction

The full-length sequence of human DPPX-L mRNA was used to perform a BLAST in the rabbit genome in Ensembl database. We selected a fragment of 417 bp with >92% identity to the human sequence, that was amplified with the same pair of specific primers from both human and rabbit cortex mRNA. The PCR product from rabbit cortex was subcloned into pcDNA3.1 using pcDNA3.1 TOPO TA Expression Kit (Invitrogen) and sequenced. Alignment of the cloned sequence with human DPPX isoforms provided a fragment of rabbit DPPX of 324 bp, corresponding to residues 1084–1408 of human DPPX-S and with a 92% sequence identity. We selected two target sequences for designing siRNA against rabbit DPPX in regions with the highest identity with the human sequence. The siRNA sequences where labeled as DPPXA (5′-CGAATGAGGGAGTATTACA-3′, two mismatches in the human sequence) and DPPXB (5′-ACACGAGGATGAAAGTGAA-3′, 100% identity with human DPPX). After using BLAST program to ensure specificity of the sequences across mammalian genomes, the two target sequences were used to generate siRNA expression cassettes (SECs) with the Silencer Express (siRNA Expression Cassette Kit, Ambion). SECs consist of a mouse U6 RNA-based polymerase III promoter adjacent to a hairpin siRNA template and a RNA polymerase terminator to facilitate high-level of siRNA expression. The SECs were generated by three consecutive PCRs using two gene-specific oligonucleotides (sense and antisense) for each SEC, designed from the target sequences with the PCR Primer Design Tool (Ambion Technical Resources). The PCR products were purified and used for transfection. A negative control SEC with limited homology to the mammalian genomes was used as control.

RNA Isolation and RT-PCR Methods

Total RNA was extracted from HEK cells mock-transfected or transfected with DPPX (the human full length or the rabbit fragment) alone or in combination with DPPX-siRNA using TRIzol Reagent (Invitrogen) and the DNA was completely degraded with DNase I (Ambion) following the manufacturer's instructions. 0.35 µg total RNA was reverse transcribed with MuLvRT (5000 U/ml) in the presence of 20 U/µl of RNase inhibitor, 50 µM random hexamers, 10× PCR buffer, 25 mM $MgCl_2$, and 10 mM mixed dNTPs at 42°C for 60 min. All reagents were from Applied Biosystems. From the same samples, 0.35 µg total RNA was used as genomic control in reverse transcription reaction in the absence of MuLv and RNase inhibitor at 42°C for 60 min.

The mRNA levels for DPPX were determined by quantitative real-time PCR (qPCR) on a Rotor-Gene 3000 instrument (Corbett Research) using ribosomal protein L18 (RPL18) expression levels as housekeeping gene. Amplification of cDNA was performed in 20 µl final volume and each reaction consisted of 10 µl Absolute QPCR SYBR mix (ABgene), 1 µl of 10 µM for each primer (MWG Biotech AG), and 1 µl cDNA. The PCR primers were designed using the Primer 3 website (http://frodo.wi.mit.edu/cgi-bin/primer3/primer3_www.cgi) and were selected to spam an intronic sequence and to recognize both human and rabbit DPPX. The primer sequences were 5′-CACGAGGATGAAAGTGAACG-3′ (forward) and 5′-TGATGGACTGGATGTTGTCG-3′ (reverse), and they amplify a 178-bp fragment. The PCR conditions were 15 min at 95°C; (15 s at 95°C, 30 s at 58°C, 20 s at 72°C) × 35 cycles and 3 min at 72°C. Fluorescence was acquired at 72°C. A melting curve was performed at the end of each experiment to ensure the specificity of the reaction and the absence of contaminating products (not depicted).

The expression levels of DPPX mRNA in CB chemoreceptor cells were determined from total RNA extracted from pooled chemoreceptor cells kept in culture during 24–48 h. Control experiments were performed in cultured cerebellar granule cells obtained from rabbit cerebellum according to previously published protocols (Liu et al., 2007) and kept in culture for 5–7 d. Electrodes made from capillary glass baked overnight at 200°C were filled with 7 µl of RNase-free water and the tip was broken to facilitate the aspiration of multiple cells. After collecting 25–50 cells (CB chemoreceptor cells or cerebellar granule cells), the contents of the pipette were ejected into a 0.2-ml eppendorf tube containing 1 µl of RNAsin (20 u/µl, Applied Biosystems) and kept at −80°C. RT was performed as indicated above, and 1–5-µl aliquots of this reaction were used for each qPCR determination. Total mRNA from rabbit hippocampus or cerebellum using TRIzol Reagent was used as the calibrator. In these groups of experiments a Cy5-labeled Taqman probe for rabbit RPL18 was used as endogenous control (Kääb et al., 2005).

In all experiments, no template controls (NTC) were included to exclude nonspecific amplification or sample contaminations. In both groups of experiments (transfected HEK cells and DPPX expression in rabbit tissues), the efficiency of the PCR reactions for the endogenous control (RPL18) and the gene of interest (DPPX) was calculated by using serial dilutions of the control samples in order to construct standard curves for both genes. As these efficiencies were similar (differences were <0.1), data were analyzed using the threshold cycle (Ct) relative quantification method (Livak and Schmittgen, 2001), so that the fold change in expression ($2^{-\Delta\Delta Ct}$) was calculated from ΔΔCt values obtained with the expression $\Delta\Delta Ct = (Ct_{DPPX} - Ct_{RPL18})_{DPPXsiRNA} - (Ct_{DPPX} - Ct_{RPL18})_{DPPX}$.

In the siRNA, for comparison between both conditions (with and without DPPX-siRNA), the mRNA amount for the transcript in the samples without siRNA, normalized to that of internal control, RPL18, was designated as the calibrator. Using the $2^{-\Delta\Delta Ct}$ method, the data in samples with DPPX-siRNA are presented as the fold change in gene expression normalized to RPL18 and relative to samples without siRNA. The same calculations were performed to quantify DPPX expression levels in rabbit CB chemoreceptor cells or cerebellar granule cells, being the hippocampus samples the calibrator in this case. To do statistical comparisons, ΔCt values obtained in each control sample, $(Ct_{DPPX} - Ct_{L18})_{Control}$, were subtracted from the mean ΔCt to provide the SE of the control group.

Electroporation of Cultured Rabbit CB Chemoreceptor Cells

Single cell electroporation was performed using modified patch-clamp techniques, following previously published models (Rae and Levis, 2002). A home-made device consisting on an operational amplifier connected to a current to voltage converter allows the supply of train pulses from −9 to +9 V through a patch pipette. The train pulses were produced using pClamp and Digidata 1200 as the pulse generator, which allows independent setting of the duration and frequency of each pulse and the total time of the train pulse delivery. The protocol used consisted of a train of 30–50 pulses, 1.5 ms long and of 6 V of amplitude. Electroporation pipettes were made from borosilicate glass capillaries (World Precision Instruments Inc.) pulled with a micropipette puller (P-97, Sutter). The pipette resistances were 20–30 MΩ when the pipette was filling with pipette solution. This solution was the internal solution used for the recording experiments to which 33 ng/µl of a plasmid DNA encoding GFP alone or in combination with 7 ng/µl

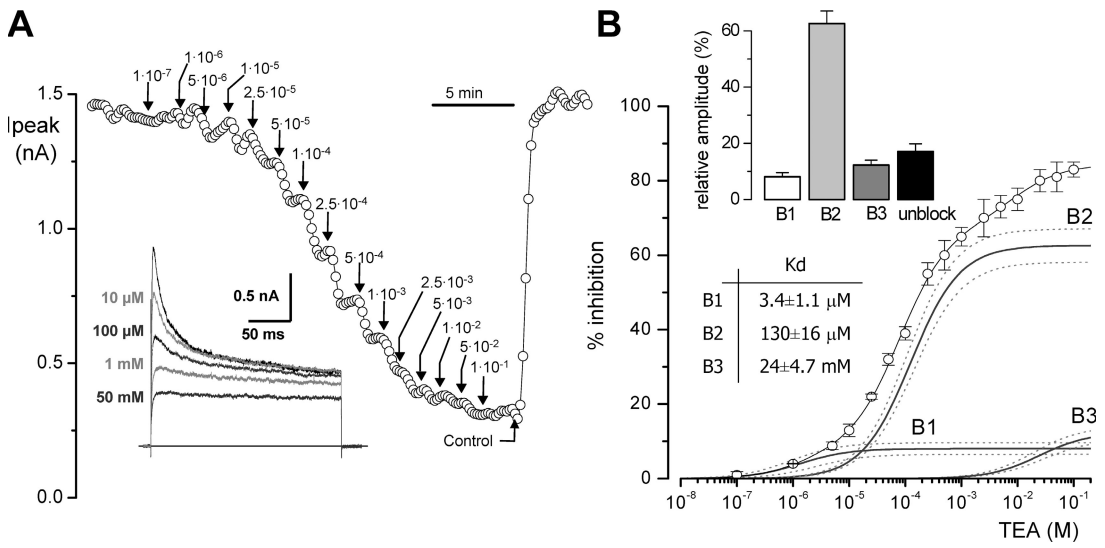

Figure 1. TEA block of transient K^+ current in rabbit CB chemoreceptor cells. (A) Representative experiment showing the decrease in the peak current amplitude in depolarizing pulses to +40 mV upon application to the bath solution of TEA at concentrations from 10^{-7} M to 10^{-1} M as indicated. Representative traces obtained in control conditions and during application of 10 µM, 100 µM, 1 mM, and 50 mM TEA are depicted in the inset of the figure. (B) TEA dose–response curve obtained with data (mean ± SEM of 9–12 individual determinations) from 12 CB chemoreceptor cells. The continuous line through the data points shows the best fit obtained with a hyperbolic function with three binding sites, with the following equation:

$$\%Inhibition = \sum_{i=1}^{i} \frac{B\max_i[TEA]}{kd_i + [TEA]},$$

where %Inhibition represents the TEA-sensitive fraction of the current and was calculated as $100 \times (I_{Control} - I_{TEA})/I_{Control}$ and $i = 3$. $I_{Control}$ was obtained by averaging peak current amplitudes before and after TEA application and I_{TEA} represents the peak current amplitude obtained by averaging several traces in the presence of the corresponding TEA concentration. The relative amplitude of these three components (B1 to B3) and the overall shape of each binding curve (±SEM) is also indicated in the figure. The inset shows the mean ± SEM of the relative amplitude of the three components (B1 to B3) and their corresponding TEA dissociation constants (Kd_1 to Kd_3) obtained from averaging the individual fits of each cell.

of DPPX or negative control SEC were added. GFP-transfected cells were recorded 24–48 h after electroporation.

Immunocytochemical Methods

Immunocytochemistry on HEK cells or isolated CB chemoreceptor cells in culture was performed as described previously (Perez-Garcia et al., 2004). In brief, carotid body cells were fixed with 4% paraformaldehyde in phosphate buffer, pH 7.5, washed in PBTx (PBS, 0.1% Triton X-100), and blocked with PBTx-2% normal goat serum. The primary antibodies, mouse anti-TH (Abcam), goat anti-Kv4.3 (Santa Cruz Biotechnology), rabbit anti-MiRP1 (Alomone laboratories), rabbit anti-DPPX (provided by E. Wettwer, Dresden University of Technology, Dresden, Germany) or goat anti-DPPX (Santa Cruz Biotechnologies), were diluted in blocking solution and incubated with the cells for 60 min at room temperature. After several washes in PBTx, cells were incubated with secondary antibodies for 30 min. The fluorescence-labeled secondary antibodies used were Alexa 488/597-conjugated anti-rabbit/mouse/goat secondary antibodies (Molecular Probes). After washes in PBS, the coverslips were mounted with Vectashield H-1000 (Vector Laboratories) with DAPI, and the cells were examined with the appropriate filters for immunofluorescence on a Nikon Eclipse 80i microscope and captured with a DXM1200C digital camera. Deconvolution was performed with Huygens Essential image processing software (Scientific Volume Imaging).

Western Blotting

48 h after transfection, the homogenized proteins from transfected and untransfected HEK 293 cells were recovered from organic phase created by addition of chloroform to TRIzol Reagent (Invitrogen, see manufacturer's protocol). Proteins, XT Reducing Agent (Bio-Rad Laboratories) and XT Sample Buffer (Bio-Rad Laboratories) were heated for 5 min at 70°C and sonicated in an ultrasonic bath, then the proteins were separated by SDS-PAGE and transferred to a PVDF membrane. After blockade with 5% nonfat dry milk in 1× PBST (PBS with 0.1% Tween 20), the membrane was incubated for 1 h with rabbit anti-DPPX at a final concentration of 1:500 in blocking solution. Then, the membrane was washed with PBST and incubated with horseradish peroxidase–conjugated secondary antibodies (1:5,000, goat anti–rabbit; Santa Cruz Biotechnology) for 1 h. The protein signals were detected with the VersaDoc 4000 Image System (Bio-Rad Laboratories) with chemiluminescence reagents (Super Signal West Pico Chemiluminescent Substrate; Pierce Biotechnology).

Kinetic Simulations

MATHCAD software (©1986–2003 Mathsoft Engineering & Education, Inc.) was used to generate simulated Kv4.3/DPPX currents by the Q-matrix method. Pulse protocols used in the simulations were the same as those used in the experiments.

RESULTS

TEA Effect on Transient K Currents from Rabbit CB Chemoreceptor Cells

We tested the effect of TEA on the native CB chemoreceptor cells by analyzing the reduction in the peak current

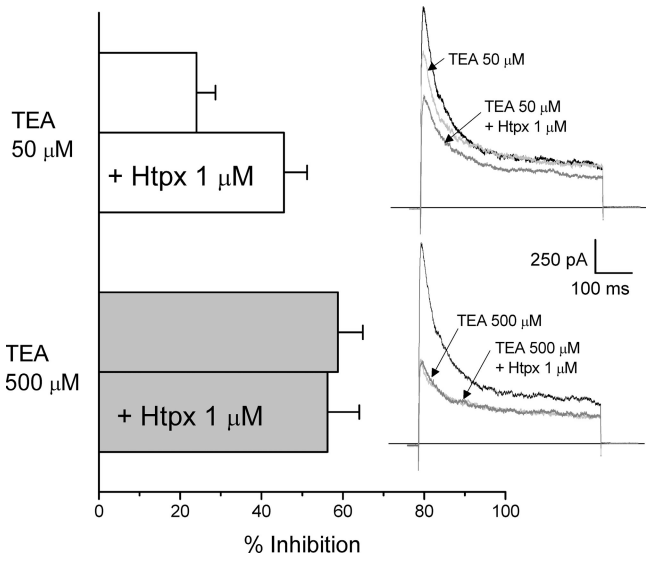

Figure 2. Occlusion by TEA of the effect of HpTx in CB chemoreceptor cells. The bar plot shows the reduction in the peak current amplitude in depolarizing pulses to +40 mV induced by the application of 50 μM TEA (white bars) or 500 μM TEA (gray bars) alone or in combination with 1 μM HpTx as indicated. Traces on the right show representative examples in each situation. Data are mean ± SEM of six cells in which the whole protocol has been applied.

amplitude in 200-ms depolarizing pulses to +40 mV in the presence of increasing TEA concentrations (from 0.1 μM to 100 mM) in the bath solution. A typical experiment is shown in Fig. 1 A. TEA inhibition of the current amplitude could be seen with concentrations as low as 1 μM, although increasing TEA up to 100 mM did not block completely outward currents. The average dose–response curve obtained in 12 different cells, where TEA effect was computed as percentage of peak current inhibition, is depicted in Fig. 1 B. Data were best fit to a hyperbolic saturation curve assuming three binding sites for TEA. Comparison of fits assuming different number of binding sites (performed with the F-test) showed a statistical difference between one- and two- and between two- and three-binding sites functions, but not between three and four-binding sites. The affinity constants obtained were 2 μM, 80 μM, and 9.16 mM, and the relative amplitudes of the three components 7.25, 60.7, and 16.4%, respectively. The isolated fitting functions for each component (B1, B2, and B3) are also depicted in Fig. 1 B. The best fit to the data from each individual cell was also obtained with the three binding-site model. The averaged fit parameters obtained in the 12 cells are shown in the inset of Fig. 1 B. The intermediate affinity component was the most abundant, representing a 62.64 ± 4.2%, while the high-affinity and low-affinity components were 8.1 ± 1.5% and 12.26 ± 1.7% of the current, respectively. The TEA-resistant fraction averaged 17.0 ± 2.7%. The dissociation constants (Kd) of the average of the fits are also indicated on the figure.

Transient outward currents in rabbit CB chemoreceptor cells have been shown to be comprised of Kv3.4 and Kv4.1/4.3 channels (Perez-Garcia et al., 2000; Sanchez et al., 2002), and both the pharmacological and kinetic profile are consistent at identifying Kv3.4 as the high-affinity TEA component. However, the intermediate-affinity (and to a lower extent the low-affinity) component is clearly a transient current representing the larger portion of the total outward current, that can be attributable to Kv4 currents, and that shows an atypical behavior with respect to TEA sensitivity. To explore more directly this extent, we investigated if selective blockers of Kv4 channels, such as heteropodatoxin-2 (Sanguinetti et al., 1997), inhibit the same channel population as submillimolar TEA concentrations. We have used 50 μM TEA to completely block the high TEA-sensitivity component, which we have previously described as the BDS-sensitive component (Kääb et al., 2005), and TEA 500 μM to block the intermediate TEA sensitivity component. According to data from Fig. 1, the fraction of the outward current resistant to 50 μM TEA and sensitive to 500 μM TEA represents most of the intermediate-affinity component. In this set of experiments (see Fig. 2), CB chemoreceptor cells were subjected to two consecutive applications of 1 μM HpTx, in the presence of 50 and 500 μM TEA, respectively. Perfusion of the cells with 50 μM TEA in the bath solution led to a 24.02 ± 4.6% reduction of the peak current amplitude, and 1 μM HpTx increased inhibition up to 46.2 ± 5.4%. However, application of 500 μM TEA completely eliminated the HpTx-sensitive current, suggesting that both drugs are acting on the same channel population. These data prompted us to explore the possible presence of Kv4 accessory subunits in rabbit CB chemoreceptor cells whose association with Kv4 channels could modulate TEA sensitivity of the heteromultimers.

Presence of Kv4 Modulatory Subunits in Rabbit CB Chemoreceptor Cells

We have used immunocytochemistry in isolated chemoreceptor cells to determine the presence, at the protein level, of several Kv4-associated subunits. Our initial approach was to explore the expression of subunits with membrane-spanning regions and extracellular domains that could be directly involved in extracellular binding of TEA to Kv4 channels, so we focused on MiRP1 and DPPX subunits. It has been suggested that in addition to its regulatory role on HERG channels, MiRP1 may serve as a regulatory subunit of I_{TO} channels in the heart (Zhang et al., 2001). However, in cultured rabbit CB cells, MiRP1 expression was found in very few cells (Fig. 3 A), and in most of the cases did not coexpress with tyrosine hydroxylase (TH, a chemoreceptor cell marker). The situation was very different for DPPX, as we found

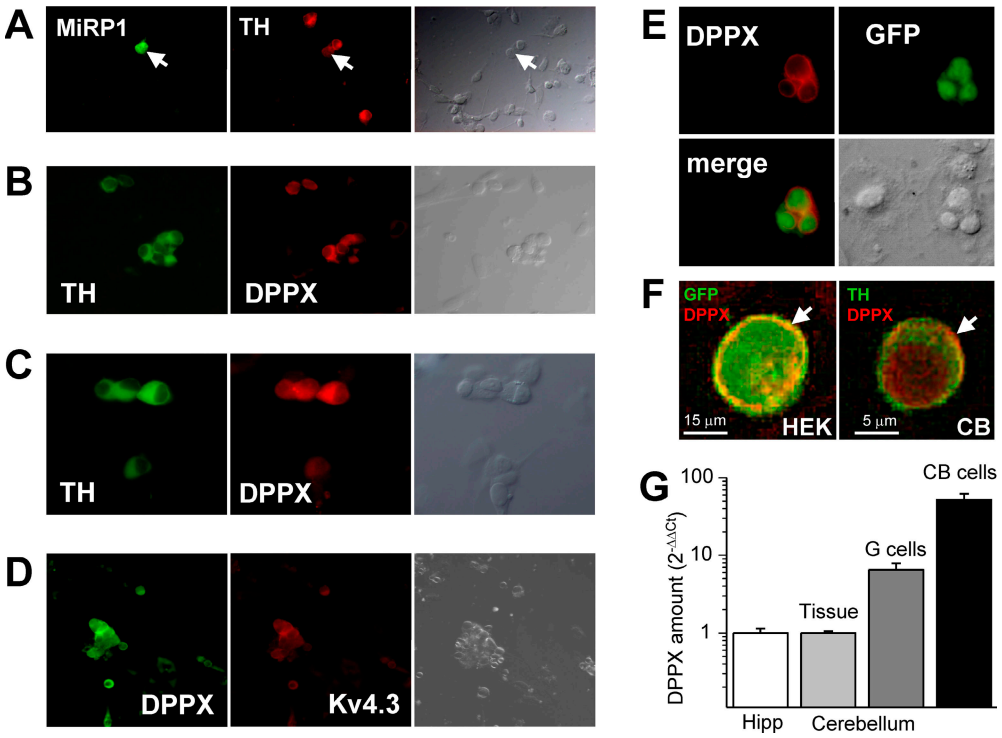

Figure 3. MIRP1 and DPPX expression in rabbit CB chemoreceptor cells. (A) The presence of MiRP1 protein in cultured CB chemoreceptor cells was explored by double labeling with anti-TH and anti-MiRP1 antibody. MiRP1-positive cells were scant and of those very few were chemoreceptor cells (as the one marked with the arrow). The corresponding transmitted light image is also shown for each field. (B) Immunofluorescence labeling of DPPX shows the expression of DPPX in every TH-positive cell (and also in some TH-negative cells). Anti-DPPX antibody provided by E. Wettwer. (C) Same results as in B were obtained with anti-DPPX antibody from Santa Cruz Biotechnologies. (D) Double labeling of CB chemoreceptor cells with anti-Kv4.3 and anti-DPPX antibodies shows an almost perfect coexpression of these two proteins, as expected if they associate in heteromultimeric channels. (E) Specificity of the DPPX antibodies was explored in HEK cells transfected with GFP+DPPX. (F) Deconvolved images showing a preferential localization of DPPX (arrows) in the surface of a Kv4.3+DPPX-transfected HEK cell (left) and a chemoreceptor cell (right). Red fluorescence corresponds to DPPX labeling, and green fluorescence corresponds to GFP (left) or TH (right) labeling. Anti-DPPX antibody from E. Wettwer was used in E and F, but the same results were obtained with the other antibody tested. (G) Real-time PCR showing the relative abundance of DPPX mRNA in CB chemoreceptor cells in primary culture. Normalized amount of DPPX mRNA in rabbit hippocampus (Hipp) was used as calibrator, and DPPX mRNA abundance in whole cerebellum (Tissue) and in cerebellar granule cells (G cells) were determined for comparisons. For details of the $2^{-\Delta\Delta Ct}$ relative quantification method see Materials and methods section. Each bar is the mean ± SEM of four to seven individual determinations.

that all TH-positive cells were stained with anti-DPPX antibody and also observed a perfect correlation with double-immunocytochemistry with antiKv4.3 and anti-DPPX antibodies (Fig. 3, B–D). The specificity of the antibodies for recognizing DPPX in immunocytochemistry was studied in HEK cells cotransfected with GFP + DPPX or GFP + DPPX + Kv4.3. In both cases we found a perfect match between GFP-expressing cells and DPPX labeling (Fig. 3, E and F). Although fluorescence with anti-DPPX does not seem to be confined to the cell membrane, deconvolution analysis of the images indicates that there is DPPX labeling at the plasma membrane (Fig. 3 F). To further confirm the presence of DPPX in rabbit CB chemoreceptor cells, qPCR experiments using SYBRgreen were performed in pooled chemoreceptor cells obtained from CB cultures, using RPL18 as housekeeping gene (Kääb et al., 2005). DPPX mRNA levels of rabbit hippocampus were used as the calibrator, and calculations were made with the $2^{-\Delta\Delta Ct}$ method as described in the methods section. We have also measured DPPX mRNA levels in cerebellum, both in the whole tissue and in pooled granule cells obtained from cultures. Our data (Fig. 3 G) shows similar expression levels of DPPX mRNA in rabbit hippocampus and cerebellum, and an almost sixfold increase when we study isolated granule neurons. However, we found much higher expression levels of DPPX mRNA in our preparation (rabbit CB chemoreceptor cells) where the quantification shows a 50-fold increase as compared with the control tissue, and almost 10 times more than in granule cells. Altogether, these data suggested that DPPX could represent a good candidate to modulate Kv4 currents in CB chemoreceptor cells.

Functional Effects of DPPX on Kv4.3 Currents

HEK-293 cells were transfected with Kv4.3 cDNA or cotransfected with DPPX and Kv4.3 cDNAs in order to study in isolation the effects of DPPX on the kinetic and pharmacology of Kv4.3 currents. Immunocytochemistry with anti-DPPX antibody was used to determine the membrane location of DPPX in transfected (GFP-positive) cells (Fig. 3, E and F). To exclude a possible association between DPPX and HEK endogenous channels we performed control experiments in cells transfected with DPPX alone. Neither the amplitude of the endogenous currents nor their kinetics were significantly altered by

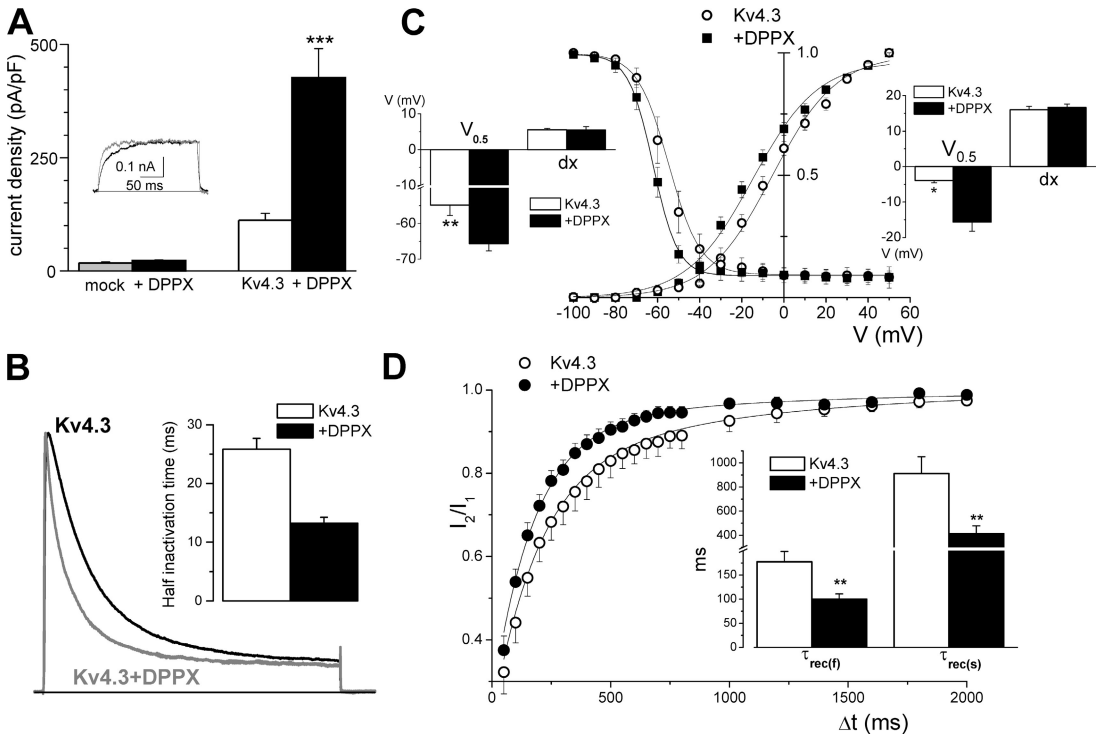

Figure 4. Effects of DPPX coexpression on the kinetics of Kv4.3 currents in HEK cells. (A) Average current density obtained in HEK cells in the four situations indicated: mock transfected (n = 8; gray bar), transfected with DPPX alone (n = 10; black bar), with Kv4.3 alone (n = 23; white bar), or with Kv4.3+DPPX (n = 47; black bars). Data are mean ± SEM, ***, P < 0.001. The inset shows traces obtained in a depolarizing pulse to +40 mV in a mock transfected cell (gray trace) or in a DPPX-transfected cell (black line). (B) Cotransfection of DPPX produced an acceleration of inactivation of Kv4.3 currents in HEK cells. The figure show normalized representative traces obtained in a Kv4.3 (black line) and a Kv4.3+DPPX transfected cell (gray trace) during 200-ms pulses to +40 mV. The speed of inactivation was quantified by analyzing the time in which the current amplitude decays to 50% of the peak amplitude (half inactivation time). The inset shows the average half inactivation time obtained in outside-out macropatches in the two conditions. n = 18 for Kv4.3 patches and n = 13 for Kv4.3+DPPX patches. (C) Normalized steady-state inactivation and conductance–voltage relationship obtained in HEK cells expressing Kv4.3 alone (open circles) or together with DPPX (closed squares). Steady-state inactivation was studied by measuring the amplitude of 500-ms pulses to +40 mV preceded by 6.5-s prepulses to potentials between −100 and +40 mV in 10-mV steps. The time between episodes was 30 s. The peak conductance–voltage relationship was calculated from the current–voltage relationship obtained in the prepulses by using the equation $G = I/(E_m - E_{rev})$, where I is the peak current, E_m is the command voltage, and E_{rev} is the reversal potential. Normalized peak conductance–voltage curves and steady-state inactivation curves were fitted using Boltzmann functions. Each point represents the mean ± SEM of seven individual determinations. The insets show the mean of the slopes (dx) and the voltages ($V_{0.5}$) for half-inactivation (left inset) or half-activation (right inset) obtained by averaging the Boltzmann fits of each individual cell. *, P < 0.05; **, P < 0.01. (D) The recovery from inactivation was studied with a two-pulse protocol in which two depolarizing pulses to +40 mV from a holding potential of −80 mV were applied with a variable interpulse interval at −80 mV, and the amplitude of the second pulse (I_2) relative to the first one (I_1) is plotted against the interpulse interval. Each point is the mean ± SEM of seven cells in each condition, and the continuous lines show the fit of the data to a biexponential function. The mean of the fast (τ_f) and slow time constants (τ_s) obtained in the individual fits are shown in the inset. **, P < 0.01.

DPPX (Fig. 4 A), suggesting a lack of association between them. When comparing the properties of cells expressing Kv4.3 alone or in association with DPPX we found that DPPX exerts a chaperone effect on Kv4.3 currents, as current density increases around fourfold in DPPX cotransfected cells (from 111.7 ± 15 to 426.7 ± 63 pA/pF, Fig. 4 A). This chaperon effect of DPPX is a lower estimate, considering that the amount of Kv4.3 plasmid in Kv4.3+DPPX-cotransfected cells was five times lower than in Kv4.3-transfected cells, and also because Kv4.3+DPPX currents in many cells had to be studied in macropatches in the outside-out configuration, as the current amplitude was too large to obtain a good voltage clamp.

We next compared the electrophysiological properties of both groups of cells. We found that DPPX increased the rate of inactivation of Kv4.3 currents (Fig. 4 B). Time to half inactivation in depolarizing pulses to +40 mV was 25.84 ± 1.86 ms for Kv4.3 and 13.23 ± 1.0 ms for Kv4.3+DPPX currents (P < 0.001). Coexpression of DPPX also produced a leftward shift in the voltage dependence of steady-state inactivation and in the conductance–voltage relationship (Fig. 4 C). Finally, in the presence of DPPX we observed an increase in the rate of recovery from inactivation (Fig. 4 D). In both groups, recovery from inactivation was best fit to a biexponential function, the fastest component being the dominant

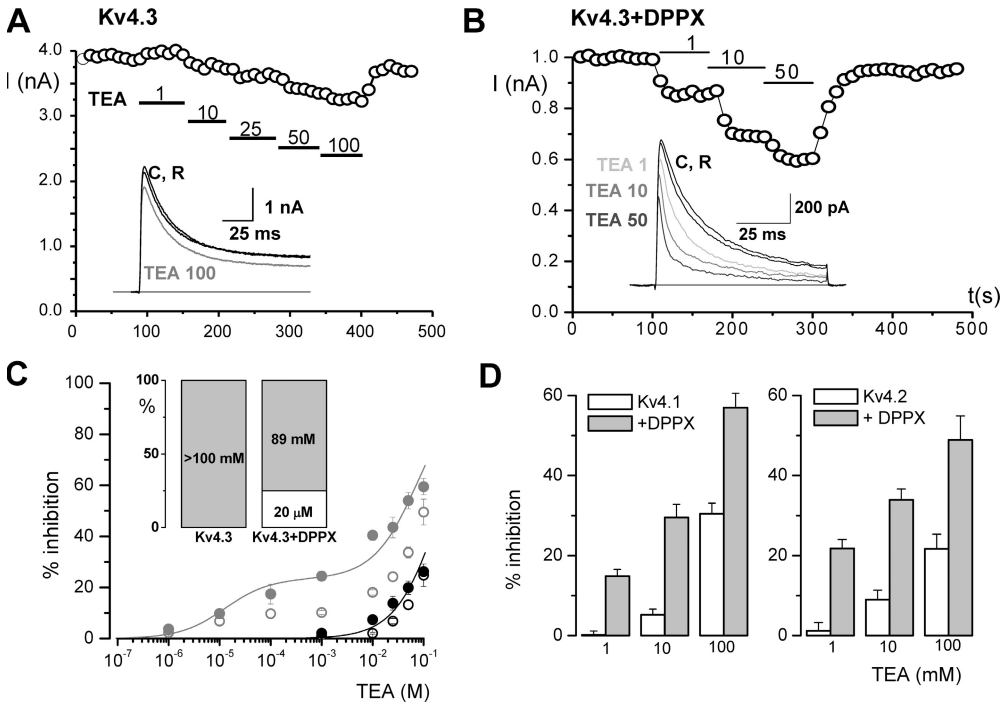

Figure 5. TEA block of Kv4.3 and Kv4.3+DPPX channels in HEK cells. The effect of TEA was determined by studying the changes in the amplitude of the currents elicited by depolarizing pulses to +40 mV upon application of increasing TEA concentrations to the bath solution. An example of the changes in the peak current amplitude of a Kv4.3 (A) and a macropatch from a Kv4.3+DPPX transfected cell (B) is plotted. Representative current traces at the indicated TEA concentrations are shown in the insets. (C) Dose–response curves for the effect of TEA on Kv4.3 (black circles) and Kv4.3+DPPX currents (gray circles). The filled symbols represent the TEA-sensitive fraction calculated as $100 \times (A_{Control} - A_{TEA})/A_{Control}$, where A is the integral of the current elicited by the depolarizing pulse. The lines represent the fit of the data to a hyperbolic function with one binding site for TEA (in the case of Kv4.3) or two binding sites in the case of Kv4.3+DPPX (see legend to Fig. 1 for equation, $i = 2$). Data points are mean ± SEM. The open symbols show the inhibitory effect of TEA on the peak current amplitude in both cases (Kv4.3 alone or Kv4.3+DPPX) calculated as in Fig. 1 B. (D) Inhibitory effect of TEA on Kv4.1 and Kv4.2 channels, alone or in combination with DPPX. The bar plots show the percent inhibition of the current integral at +40 mV obtained at three different TEA concentrations (1, 10, and 100 mM). Data are mean ± SEM of 9–12 cells in each condition.

kinetic one. The time constants of both components were significantly decreased upon DPPX coexpression, from 177 ± 12 to 100.07 ± 10.8 ms (fast component) and from 911 ± 58 to 413 ± 65 (slow component) in Kv4.3 and Kv4.3+DPPX currents, respectively.

External TEA Block of Kv4.3+DPPX Currents

Next we explore TEA sensitivity of these two groups of cells (Kv4.3 and Kv4.3+DPPX-expressing cells). In Kv4.3-expressing cells we found that, as previously described, external TEA concentrations as high as 100 mM weakly inhibited Kv4.3 currents (around 15% in the cell shown in Fig. 5 A), causing little or no effect on current kinetics. However, the effect of TEA was remarkably different in cells coexpressing DPPX (Fig. 5 B). First, there was a clear increase in TEA affinity, so that the reduction in the peak current amplitude could be seen at low TEA concentrations and the currents were blocked almost 50% by 50 mM TEA. Dose–response curves of the effect of TEA on current amplitude are shown in Fig. 5 C. TEA inhibition was calculated in two different ways: as the reduction in the peak current amplitude (open symbols) or by subtracting the current integral of the depolarizing pulse calculated both in control and in the presence of the indicated TEA concentrations (filled symbols). These two different methods provided similar results in the case of Kv4.3 currents, but not when studying Kv4.3+DPPX currents. For Kv4.3 currents, the best fit was obtained by assuming a single TEA-binding site of low affinity (estimated IC50 of 322 mM). In the presence of DPPX, the optimal fit of the data obtained by the integral method came by assuming two TEA-binding sites, one of high (apparent Kd ∼20 μM) and another of low affinity (apparent Kd ∼89 mM). Each point in the graph of Fig. 5 C represents the mean of 25–80 individual determinations, as a high variability was observed when studying TEA block on the Kv4.3+DPPX currents. Nevertheless, in spite of the variability, in the presence of DPPX, the currents were always more sensitive to TEA than homomeric Kv4.3 currents.

Similar effects of DPPX on TEA sensitivity could be observed with the other two members of the Kv4 subfamily. Fig. 5 D shows the inhibition of the current integral obtained with three TEA concentrations (1, 10, and 100 mM) in HEK cells expressing Kv4.1 or Kv4.2 alone (white bars) or together with DPPX (gray bars). A remarkable increase in TEA sensitivity was observed in both cases in the presence of DPPX, the effects of TEA on Kv4.1 and Kv4.2 being very similar to that observed for Kv4.3 (Fig. 5 C).

Effect of TEA on the Kinetics of Kv4.3+DPPX Currents

In addition to the inhibition of the peak current amplitude, the changes in the macroscopic kinetics of Kv4.3+DPPX currents in the presence of TEA have been

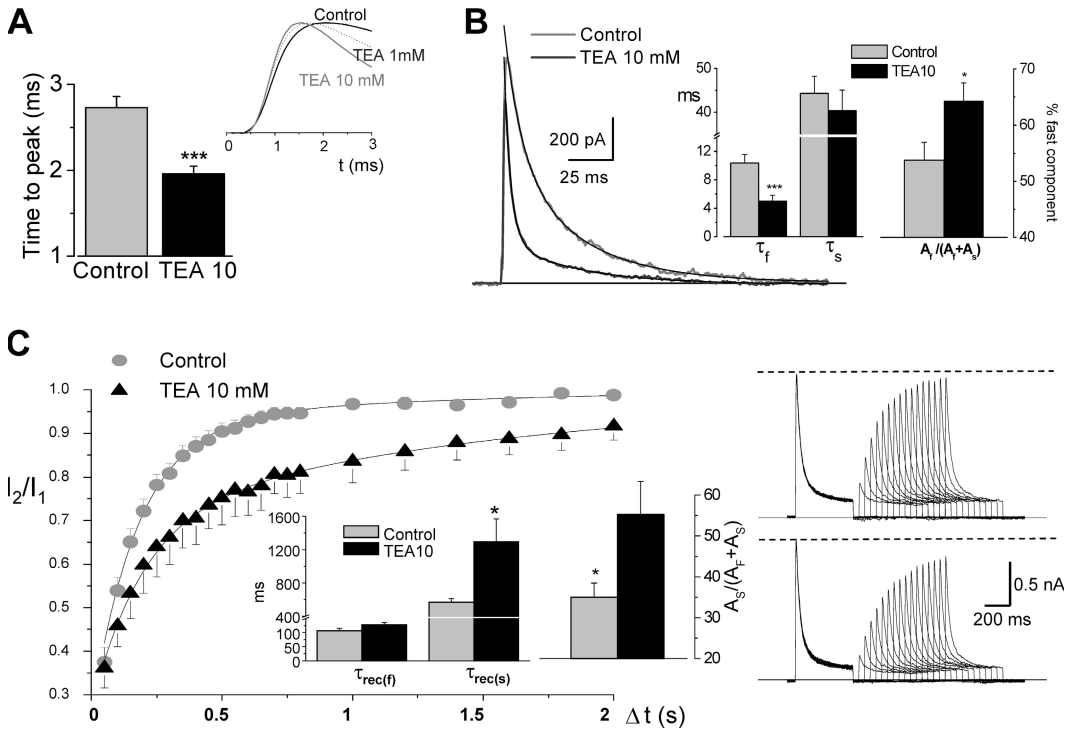

Figure 6. Modulation by TEA of the kinetics of Kv4.3+DPPX channels. (A) Speed of activation was studied in depolarizing pulses to +40 mV in outside-out macropatches, and was calculated as the time to peak current amplitude. The traces in the figure show normalized currents obtained in one representative cell in control (black line) and in the presence of 1 mM TEA (dotted line) and 10 mM TEA (gray line). The bar plot shows the mean data from 15 patches in control and in the presence of 10 mM TEA. ***, $P < 0.001$ for paired data. (B) The time course of inactivation of the current elicited in 200-ms depolarizing pulses to +40 mV was fitted to a biexponential function both in control and in the presence of TEA (10 mM). The figure shows two representative traces from a macropatch together with their corresponding fits. The bar graphs display the inactivation time constants (τ_s and τ_f) and the relative amplitude of the fast component obtained in control and in the presence of 10 mM TEA. Mean ± SEM of 14 cells. *, $P < 0.05$; ***, $P < 0.001$ for paired data. (C) Recovery from inactivation at −80 mV in the presence of 10 mM TEA determined with the same double pulse protocol described in Fig. 3 D. The two time constants ($\tau_{rec(s)}$ and $\tau_{rec(f)}$) and the proportion of the slow component A_s, are the mean ± SEM of the individual fit of five Kv4.3+DPPX-transfected cells in both conditions (control and 10 mM TEA). *, $P < 0.05$. Representative traces obtained in a cell in control conditions (top traces) and in the presence of TEA 10 mM (bottom traces) are also shown in the right panels.

explored with more detail. At low (1–10 mM) TEA concentrations, time to peak is shorter (Fig. 6 A) and inactivation is faster (Fig. 6 B). We measured the time at which half of the current inactivates ($t_{0.5}$) at +40 mV in 15 outside-out patches and the values obtained were 14.96 ± 1.29 in control and 5.25 ± 0.97 in the presence of 10 mM TEA ($P < 0.001$). The time course of inactivation was fitted to a biexponential function both in the absence and in the presence of 10 mM TEA. In all cases studied ($n = 15$), TEA application leads to a marked reduction in the fast time constant (from 10.35 ± 1.2 to 5.00 ± 0.8 ms) without significant changes in the slow time constant, together with an increase in the proportional amplitude of the fast component of the current (Fig. 6 B).

As TEA induced changes in the time course of inactivation, we explored whether the recovery from inactivation was also modified (Fig. 6 C). Inactivation was induced by a 500-ms depolarizing pulse to +40 mV, and a second depolarization to +40 mV was used to determine the fraction of channels that recovered after a variable interval at −80 mV. Recovery from inactivation of Kv4.3+DPPX channels was clearly slowed down in the presence of 10 mM TEA. The time course of this recovery was fitted to a biexponential function, and the comparison of the fit of individual cells in both conditions indicated that application of TEA increased both the relative amplitude of the slow component (A_s) and the slow time constant ($\tau_{rec(s)}$), as shown in the bar graphs in Fig. 6 C.

We also studied the effect of TEA on the voltage dependence of activation and inactivation of Kv4.3+DPPX channels (Fig. 7 A). The peak conductance–voltage relationship was described by first-order Boltzmann functions, and we did not observe any significant changes in the function parameters in the presence of 10 mM TEA. However, the results were not the same when analyzing the steady-state inactivation, as 10 mM TEA produced a small (∼6 mV) but significant hyperpolarizing shift with no changes in the slope of the curve. This change in the steady-state inactivation curve could be explained by an increase in the proportion of closed-state inactivation

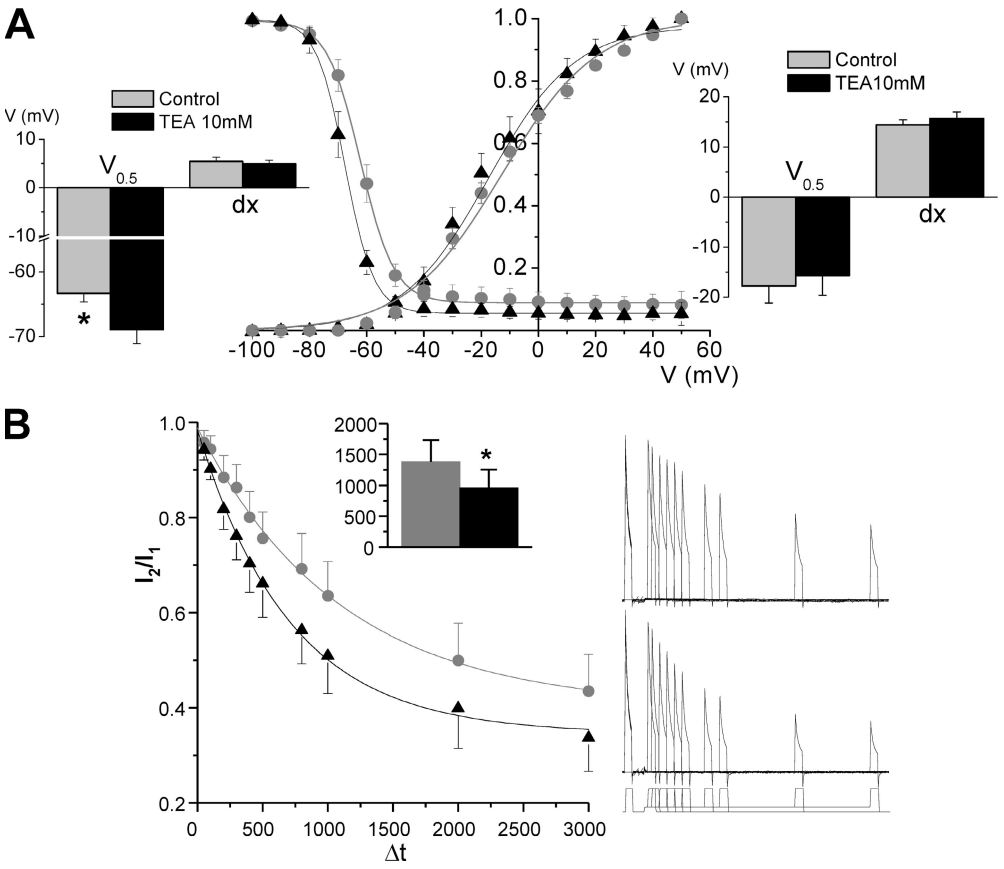

Figure 7. TEA affects steady-state properties of Kv4.3+DPPX currents. (A) Voltage dependence of peak conductance and steady-state inactivation before (gray circles) and after 10 mM TEA application (black triangles). The curves were obtained and analyzed as described in Fig. 4 C. The bar plots show the data obtained from averaging the midpoint ($V_{0.5}$) and the slope (dx) of the Boltzmann fits of each individual cell for steady-state inactivation (left) and peak conductance–voltage relationship (right). $n = 7$ cells in each group; *, $P < 0.05$. (B) Time course of the closed-state inactivation of Kv4.3+DPPX channels before and after application of 10 mM TEA. Examples of the protocol used and the current traces obtained in both conditions are shown in the right panels of the figure. In brief, a 100-ms depolarizing pulse to +40 mV from a holding potential of −80 mV was delivered to obtain the control current, and this pulse was followed to a return to −80 mV during 6 s to allow full channels recovery. After this, the voltage was stepped to a variable length prepulse potential of −55 mV before depolarizing again to +40 mV during 100 ms to determine the fraction of available channels. The normalized relationship of the peak current amplitude in the two depolarizing pulses (I_2/I_1) is plotted against the duration of the prepulse, and a single exponential function was used to fit the data. The inset shows the mean time constants obtained in the individual fits of the cells before and after TEA application. *, $P < 0.05$ for paired data; $n = 5$ cells.

in the presence of TEA, so we explore this possibility with the protocol shown in Fig. 7 B. The time course of closed-state inactivation was measured at voltages closed to the $V_{0.5}$ for inactivation under steady-state conditions, and could be described by a single exponential fit. Measurements of the preopen closed-state inactivation in the presence of 10 mM TEA show a decrease in the time constant (from 1406 ± 350 to 952 ± 302 ms). Altogether, these experiments indicate that TEA blockade of Kv4.3+DPPX channels not only reduces current amplitude but also induces changes in their inactivation kinetics. These changes could be mediated at least in part by the acceleration of the rate of closed-state inactivation.

DPPX Contribution to Transient Outward K^+ Currents in Chemoreceptor Cells

To determine whether TEA sensitivity of transient outward currents in rabbit CB chemoreceptor cells was in fact due to the presence of Kv4/DPPX heteromultimers, we studied the effects of functional suppression of DPPX on the kinetics of the native currents by using siRNA against rabbit DPPX.

siRNA validation was performed in HEK cells that were either mock transfected (control) or transfected with rabbit or human DPPX alone or in combination with siRNA against DPPX. The reduction in the expression of DPPX upon siRNA transfection was evaluated both at the mRNA (quantitative PCR) and protein (Western blot) levels (Fig. 8 A). In both cases, a significant reduction in the expression of DPPX was obtained in the presence of siRNA. However, of the two different siRNA SECs designed (see Materials and methods), DPPXB was more efficient at decreasing both human and rabbit DPPX mRNA levels. Due to this observation (predictable in the case of the human gene, as we did not have perfect sequence match, but unexpected for the rabbit one) only DPPXB siRNA has been used to induce RNAi in the native tissue.

After this validation, we studied the functional effects of DPPX down-regulation in rabbit CB chemoreceptor cells, introducing siRNA in the cells by using single-cell electroporation and analyzing the magnitude of the currents and their kinetics. For comparisons we used three groups of control cells: untransfected cells, GFP-transfected cells, and cells transfected with the siRNA

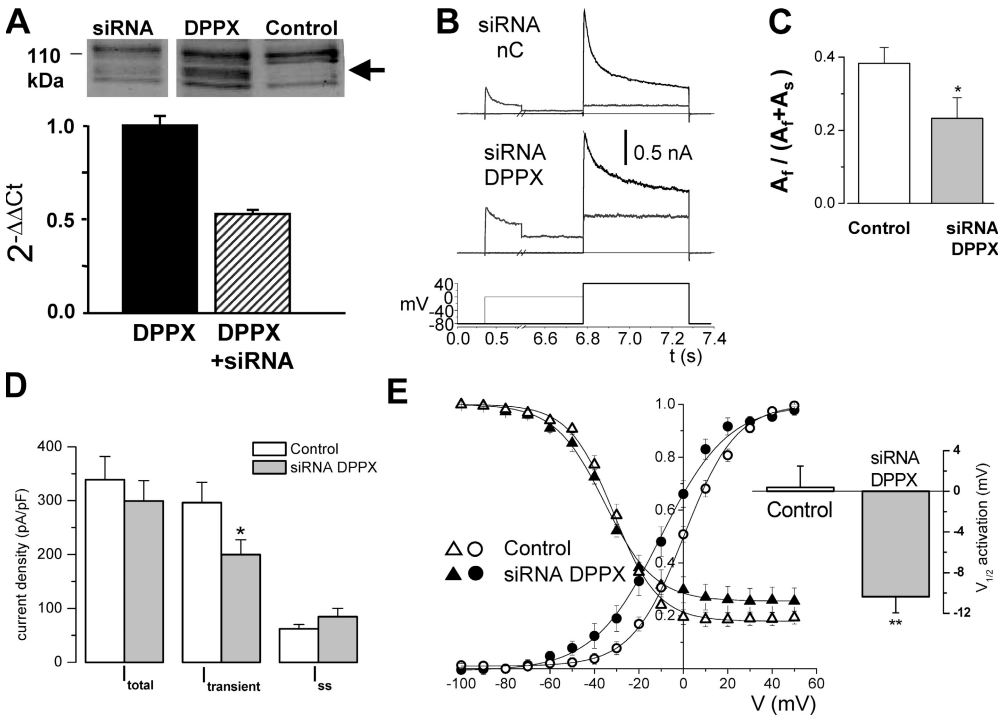

Figure 8. Functional contribution of DPPX to transient outward K^+ currents of rabbit CB chemoreceptor cells. (A) Validation of siRNA DPPX was performed, quantifying the amount of DPPX protein by Western blot and the amount of DPPX mRNA by real-time PCR. The figure shows a Western blot of lysates from HEK cells untransfected (control lane) or transfected with DPPX alone (DPPX) or DPPX+DPPX siRNA (siRNA lane), probed with anti-DPPX antibody. The arrow indicates the estimated molecular weight of DPPX protein. The reduction of the levels of DPPX mRNA was determined by qRT-PCR and analyzed with the $2^{-\Delta\Delta Ct}$ method as described in the Materials and methods section. Total mRNA was extracted from HEK cells transfected with rabbit DPPX alone or in combination with DPPX siRNA as indicated in the figure. (B) Currents recorded from two individual CB chemoreceptor cells after electroporation of GFP + negative control siRNA (siRNA nC) or GFP+DPPX siRNA (siRNA DPPX). In both cases, the currents were elicited with the voltage protocol shown at the bottom, in which 500-ms depolarizing steps to +40 mV follow 6.5-s prepulses to two different potentials, −80 mV (thicker trace) and 0 mV (thinner trace). The difference between the current amplitude at +40 mV in these two pulses is defined throughout the paper as the transient outward current. The black thick line shows the fit of the currents to a double-exponential function. (C) Inactivation fitting parameters obtained in both conditions (control and siRNA cells) indicate a significant change in the relative amplitudes of the two components of inactivation, A_f and A_s. The bar plot shows the relative proportion of the fast component. Data are mean ± SEM of 8–10 cells in each group; *, $P < 0.05$. (D) Peak current densities recorded in control or siRNA DPPX electroporated cells were obtained with the two pulse protocol described in B. I_{total} represents the peak current amplitude at +40 mV after the −80-mV prepulse, $I_{transient}$ was calculated as indicated above, and I_{ss} is the current amplitude at +40 mV after the 0-mV prepulse. *, $P < 0.05$, $n = 10$ cells in each group. (E) The normalized steady-state inactivation curves and the conductance–voltage curves from the two groups of cells were obtained and constructed as described in Fig. 4. Lines represent the best fit of the data to Boltzmann functions. Each point is the mean ± SEM of 8–10 determinations. The bar plot shows the differences in the $V_{0.5}$ for activation obtained from the individual fit of the cells in both groups.

negative control. We did not observe any differences between these three groups of controls, so control data have been pooled. Transient outward currents were studied with a two-pulse protocol (Fig. 8 B), in which the currents were elicited upon depolarization to +40 mV following 6.5-s prepulses to two different potentials, −80 mV (to obtain the fully primed current), and 0 mV (to inactivate the transient component). Thus, transient or inactivating current was defined as the difference between the current elicited by the two pulses. Fig. 8 B shows representative traces obtained in cells electroporated with the siRNA negative control and siRNA DPPX. We observed a slower time course of inactivation in the siRNA DPPX-transfected cells, and the fit of the data to a biexponential decay function indicated that siRNA DPPX induced a decrease in the amplitude of the fast component of the current (Fig. 8 C) without significant changes in the time constants (not depicted). Also, although the total outward current density of the cells transfected with siRNA DPPX was unchanged, we found a significant reduction in the proportion of the transient component of the current (Fig. 8 D), which is in agreement with the well-known chaperone function of DPP proteins on Kv4 currents (Nadal et al., 2003; Jerng et al., 2005). There was also an increase in the density of noninactivating current (Iss in Fig. 8 D) that was not statistically different. The study of the voltage dependence of activation and inactivation of CB chemoreceptor cells (Fig. 8 E) indicated that down-regulation of DPPX did not modify inactivation parameters but produced a marked and significant shift of the activation curve to hyperpolarizing potentials, without changing its voltage dependence, as the slope values were similar in both groups. This shift in the activation curve is also evident in the example shown in Fig. 8 B; in spite of the current amplitude at +40 mV being the same in the two cells shown (control and siRNA DPPX), the current amplitude in the 0 mV prepulse is clearly bigger in the siRNA DPPX cell.

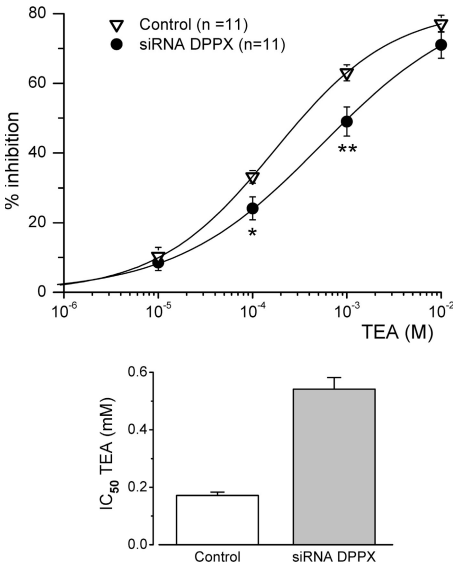

Figure 9. Effect of DPPX down-regulation on the TEA sensitivity of the transient K^+ current of rabbit CB chemoreceptor cells. The effect of TEA is represented as percentage of inhibition, and was calculated from the reduction in the peak current amplitude in depolarizing pulses to +40 mV as described in Fig. 1. Control (open triangles) represents pooled data from untransfected, GFP-electroporated, and GFP+ negative control siRNA-electroporated CB cells. Each point is the average of 11 cells in each group. The continuous lines show the fit of the data to a hyperbolic function with one binding site for TEA. *, $P < 0.05$; **, $P < 0.01$. The estimated IC50 for TEA was calculated from the average of the B_{max} values obtained from the fit of each individual cell and is shown in the bar plot on the right.

Effect of TEA on CB Chemoreceptor Cells Transfected with siRNA DPPX

Once we obtained functional evidence of DPPX down-regulation in chemoreceptor cells, we explored if there was some effect on the TEA sensitivity of the transient current. In each cell studied, we applied four different TEA concentrations (from 10 μM to 10 mM) and we normalized the reduction in the peak current amplitude observed in depolarizing pulses to +40 mV. The dose–response curves obtained are shown in Fig. 9. We found a significant reduction of TEA sensitivity in siRNA DPPX–transfected cells in the intermediate range of TEA concentrations (0.1 and 1 mM) with no changes at lower and higher concentrations. The fit of the data to a hyperbolic function shows that down-regulation of DPPX leads to a threefold decrease in the TEA affinity of the current (half inhibitory concentration of 189.76 ± 13.44 μM in control cells versus 540.96 ± 40.84 μM in siRNA DPPX–transfected cells). These data support the conclusion that the modulatory effects of DPPX on Kv4 cloned channels can also be observed in native systems.

DISCUSSION

The data presented in this work allow us to propose that the sensitivity to TEA of the Kv4 channels that largely contributes to the transient outward K^+ currents of rabbit CB chemoreceptor cells is related to the presence of DPPX accessory subunits in these cells. These findings provide an explanation to our previous observation regarding TEA sensitivity of rabbit CB K_{O2} and are also relevant to understand the contribution of DPPX to the functional properties of transient K^+ currents in this preparation; moreover, the data obtained in the heterologous expression system indicate that the modulatory effect of DPPX increasing TEA sensitivity of Kv4/DPPX heteromultimers could be a more general feature operating in many other preparations.

Native Kv4 channels are associations of pore-forming subunits and auxiliary subunits. The first class of physiologically important Kv4 auxiliary subunits, KChIPs, have been shown to increase current density and also to alter gating of associated channels, by slowing inactivation and facilitating recovery from inactivation (An et al., 2000; Takimoto et al., 2002; Patel and Campbell, 2005). Despite the fact that the same Kv4 subunits are responsible for neuronal and cardiac transient K^+ currents, inactivation of the current between the two cell types significantly differs, and it has been proposed that the presence of DPPX protein in neurons can account for these differences (Nadal et al., 2003). Interaction with DPPX facilitates inactivation of Kv4 channels and also causes changes in other gating properties such as shifts in voltage dependence of activation and inactivation to more negative potentials and facilitation of recovery from inactivation (Nadal et al., 2003). However, in the light of recent findings indicating that DPPX is also expressed in human heart, where it can also contribute to the kinetic properties of I_{TO} (Radicke et al., 2005b), it has been proposed that both DPPX and KChIP simultaneously interact with Kv4 proteins to form ternary complexes, so that differential expression of the members of these two families of auxiliary subunits controls electrophysiological properties of excitable cells. The tissue-specific assembly of the Kv4 multiproteic complex could also explain TEA sensitivity of Kv4 channels in rabbit CB chemoreceptors. It has been proposed that both the relative abundance of DPPX as well as the cell-specific expression of the DPPX splice isoforms could confer Kv4 channels with differential modulation at various levels. In this regard, it is noteworthy that the expression levels of DPPX are 10 times higher in CB chemoreceptor cells than in cerebellar granule cells, a preparation in which DPPX has been found to be prominently expressed (Nadal et al., 2003, 2006). This abundance of DPPX is also a common aspect between CB cells and the heterologous expression system, in which an excess of the accessory subunit is aimed. However, our data in CB chemoreceptor cells do not fully recapitulate the effects described in the heterologous system, as the modulatory effect of TEA on the native currents do not seem to involve clear kinetic changes. Although

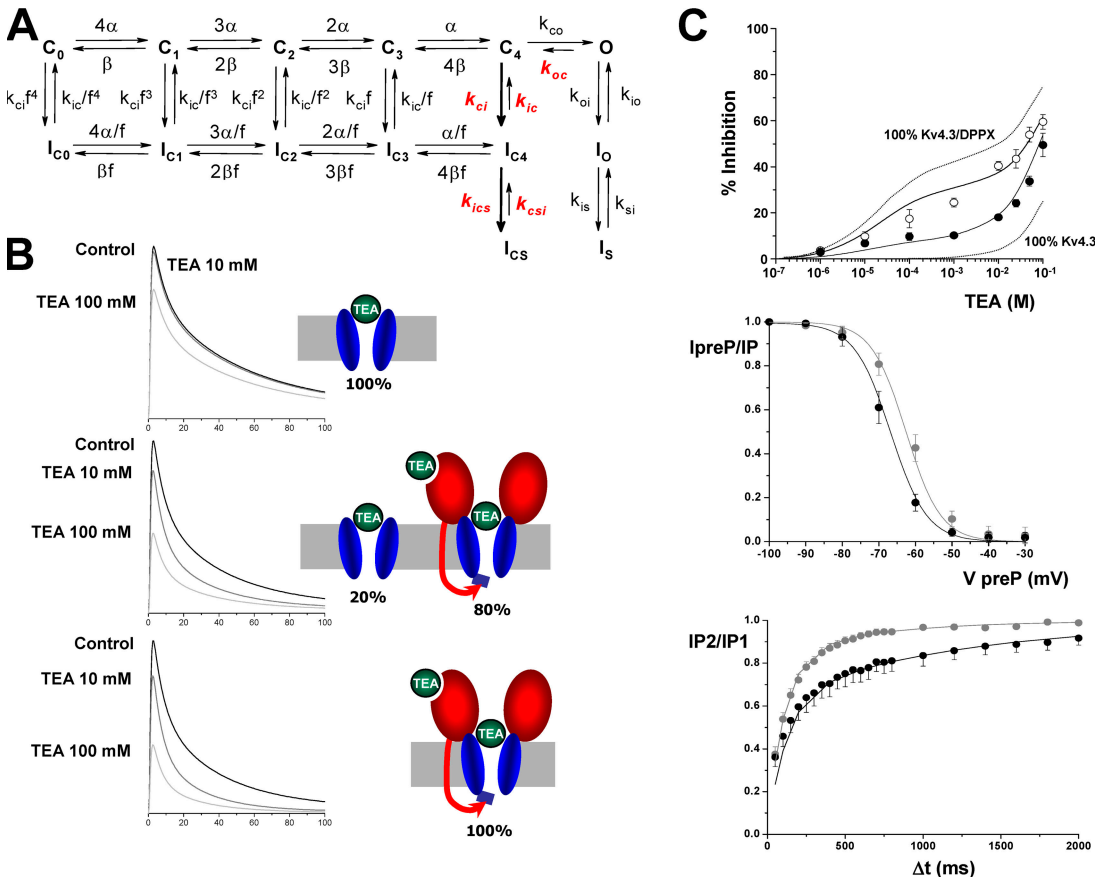

Figure 10. Model describing the effects of TEA on Kv4.3+DPPX channels. (A) The kinetic state diagram has been constructed on the basis of previously published models for Kv4 channel inactivation, the rate constants in red being the ones modified by TEA. The diagram includes inactivation both from the preopen closed states ($C_n \rightarrow I_{Cn}$) and from the open state ($O \rightarrow I_O$). From the I_{C4} and I_O inactivated states the channel also accesses deeper inactivated states (I_{CS} and I_S). Transitions between states are represented by arrows, and the values of the simulation parameters are shown in Table I. (B) Simulation with a pulse protocol as the one shown in Fig. 5, in control conditions or in the presence of TEA 10 or 100 mM. The three panels represent different proportions of Kv4.3 homotetramers and Kv4.3/DPPX heteromultimers, as depicted in the cartoons. (C) Simulations of the dose–response curve for TEA block (top graph), the steady-state inactivation curve (middle graph), and the recovery from inactivation (bottom panel) obtained with the proposed model, with 80% of Kv4.3 complexes as Kv4.3/DPPX heteromultimers. The continuous traces represent model predictions and the scatterplots the experimental data. In the dose–response curve graph, the experimental data show the inhibition by TEA of both peak current amplitude (black circles) and current integral (white circles). The dotted lines represent the predictions of the model in the two limiting possibilities, either 100% of Kv4.3 homotetramers or 100% Kv4.3/DPPX heteromultimers. In the two bottom graphs, control data (and predictions) are in gray and data in the presence of TEA (10 mM) are plotted in black traces.

the presence of other non-Kv4 channels contributing to the total transient outward current in CB cells could make these effects inconspicuous, it is also conceivable that the different molecular composition of the Kv4 complexes in the two systems studied can account for the differences in the effect of TEA in both preparations. As an example, it is clear that the values for half inactivation of the currents are clearly different in both systems (compare Fig. 4 C and Fig. 8 E); moreover, this parameter is modified by coexpression with DPPX in HEK cells while in CB chemoreceptor cells we did not see significant changes when cells are electroporated with siRNA against DPPX. As previously reported (Jerng et al., 2005), these parameters are very dependent on the expression system and the molecular structure of the Kv4 complexes. These authors find significant differences in the absolute values depending on the expression system (*Xenopus* oocytes or CHO cells). Also, by coexpressing Kv4.2 channels with different combinations of accessory subunits (including KChIP and DPPX or DPPY) they conclude that DPP proteins produces a leftward shift in the steady-state inactivation curve of Kv4 channels (similar to what we observed in HEK cells, see Fig. 4), but this effect disappears when the channels are ternary complexes with KChIP, so that the values for half inactivation of Kv4.2+KChIP+DPPY (or DPPX) channels are not different from the values for Kv4.2 homomultimers. These observations can provide a plausible explanation from the data presented here, as we have preliminary data demonstrating the colocalization

TABLE I

Model Rate Constants

Rate Constants	Kv4.3	Kv4.3/DPPX	Kv4.3/DPPX-TEA
s^{-1}	*G0*	*G1*	*G2*
α_0	550	550	550
β_0	9	5	9
k_{co}	500	600	600
k_{oc}	1100	1100	990
k_{oi}	200	200	200
k_{io}	90	90	90
k_{ci}	30	60	120
k_{ic}	0.1	0.2	0.16
k_{is}	15	15	15
k_{si}	7.5	7.5	7.5
f	0.3	0.3	0.3
k_{ics}	2.5	1	3
k_{csi}	1.4	1.5	0.75

The model has been modified from Bähring et al. (2001). The voltage-dependent rates are of the form $\alpha = \alpha_0 \cdot \exp[z_a V/(RT/F)]$ for the forward rates and $\beta = \beta_0 \cdot \exp[z_b V/(RT/F)]$ for the backward rates, where α_0 and β_0 are the rates at 0 mV and z_a and z_b are the equivalent charges moving up to the transition state. Channel opening and closing are defined by k_{co} and k_{oc}, respectively, open-state inactivation by k_{oi} and k_{io}, and closed-state inactivation by k_{ci} and k_{ic}. A deep-inactivated state, defined by k_{ics} and k_{csi}, has been introduced to reproduce the biexponential recovery from inactivation. All closed states are connected to inactivated states via k_{ci} and k_{ic}. The coupling of activation and inactivation is defined by an allosteric factor *f*. Transition leading from I_O to I_S is defined by k_{is} and k_{si}. Column *G0* represents the gating model for Kv4.3 homotetramers, *G1* for Kv4.3/DPPX heteromultimers, and *G2* the gating of these heteromultimers at saturating TEA concentrations of the high affinity binding site. Total conductance as a function of TEA concentration and the relative contribution of homo and heteromultimers are computed with the following expression:

$$GT = r \cdot \left[G1 \cdot \left(1 - \frac{TEA}{TEA + Kd1} \right) + G2 \cdot \left(\frac{TEA}{TEA + Kd1} \right) \right] \cdot \left(1 - \frac{TEA}{TEA + Kd2} \right) + (100 - r) \cdot G0 \cdot \left(1 - \frac{TEA}{TEA + Kd3} \right),$$

where *Kd1*, *Kd2*, and *Kd3* are the affinity dissociation constants obtained experimentally, and *r* represent the percentage of Kv4.3/DPPX present in the membrane.

of KChIP proteins in TH-positive and Kv4.3-labeled CB cells (unpublished data).

Inactivation of Kv4 channels is a complex multi-exponential process that can proceed from both the closed and open states of the channel (Jerng et al., 1999; Bahring et al., 2001; Beck and Covarrubias, 2001). The changes in inactivation gating induced by coexpression of DPPX (or DPPY) can be explained by an allosteric model of Kv4 gating with preferential closed-state inactivation, so that the leftward shift in steady-state inactivation of Kv4 channels in the presence of DPPX or DPPY would reflect the dominance of entry into closed-state inactivation over recovery from inactivation (Jerng et al., 2004a,b). The modulatory effects of DPPX on Kv4.3 currents we present in this work (HEK cells) are similar to those previously described in other expression systems such as *Xenopus* oocytes and CHO cells. We found a chaperone effect of DPPX on Kv4.3 currents, together with an increase in the rate of inactivation, a hyperpolarizing shift in the voltage dependence of activation and inactivation and an increase in the rate of recovery from inactivation of Kv4.3+DPPX currents (Fig. 4). In addition to these effects, Kv4.3+DPPX heteromultimers are clearly more sensitive to externally applied TEA (Figs. 5 and 6). The best fit of the dose–response curve of the inhibitory effect of TEA on Kv4.3+DPPX currents was obtained by assuming a two-binding site model, which implies that DPPX creates a new, high-affinity, TEA-binding site. There is also an apparent increase in the affinity of the previously existent low-affinity binding site on Kv4.3 channels, although we do not know whether this change is significant as this binding site cannot be sufficiently resolved to provide the actual binding affinities. Interestingly, binding of externally applied TEA to this new high-affinity site that appears in the presence of DPPX leads to some marked kinetic effects, such as the acceleration of the inactivation rate, the shift in the voltage dependence of inactivation, and the slow down of the recovery from inactivation (Figs. 6 and 7). These experimental data can be reproduced by previously published kinetic models of Kv4 channels, just assuming that binding of TEA to the new high-affinity site facilitates transitions leaving closed states toward both inactivated and open states (Fig. 10). We have used the "allosteric model of inactivation" previously proposed by Bärhing and coworkers (Bähring et al., 2001; see also Beck and Covarrubias, 2001; Jerng et al., 2004b) as it was able to adequately simulate the gating of Kv4.3+DPPX channels in our preparation, with slight modifications of the published rate constants. However,

while in all these models the time course of the recovery from inactivation is monoexponential, in our experimental data the best fit was always obtained with a bi-exponential function (see Fig. 4), even though the slow component represented <15% of the total amplitude. One of the most remarkable kinetic effects of TEA on Kv4.3+DPPX channels is to increase the proportion of this slow component up to 50% of the total amplitude. For this reason, we have included a deep-inactivated state (I_{CS}) from the closed-inactivated state I_{C4}. Regarding the dose–response curve to TEA, we have observed a high variability between cells in the proportion of the high-affinity component. Although this component represents 25% in the average data (see Fig. 5 C), in some cells it was as high as 60%. We speculate that this variability could reflect the presence of different channel populations (with and without DPPX, or even with different stoichiometric ratio of DPPX), and this has been taken into account in the model, as could also explain differences in DPPX effect between different native tissues. The model assumes that Kv4.3 homotetramers and Kv4.3/DPPX heteromultimers can coexist in the membrane in a variable proportion. Kv4.3 homotetramers have a single TEA binding site, and binding produces a channel pore block. Kv4.3/DPPX heteromultimers have two binding sites, and binding to the high-affinity site induces a kinetic change while binding to the low-affinity site produces a channel pore block. The Kds of TEA binding used in the model are those obtained experimentally. The model best reproduces the average dose–response curve, either measuring peaks or areas, when considering a proportion of 80% of heteromultimers (Fig. 10 B). Computer simulations with this model indicate that the kinetic changes observed in Kv4.3+DPPX channels in the presence of TEA concentrations that saturate the high-affinity site (>1 mM) can be adequately reproduced by simultaneously accelerating transitions k_{Ci} and k_{iCS} and decreasing the opposite transitions k_{iC} and k_{CSi}. A decrease in k_{OC} is also necessary to simultaneously fit the kinetic changes and the effect on peak currents. These changes accelerate Kv4.3+DPPX closed-state inactivation, produce a shift in the voltage dependency of inactivation, and slow down the time course of recovery from inactivation (see Fig. 10 C). Rate constants used in the model (Table I) also reproduce the effect of DPPX on Kv4.3 steady-state inactivation and recovery of inactivation (not depicted). The model does not adequately reproduce the time course of closed-state inactivation obtained experimentally (Fig. 7 B), although it reproduces the TEA-induced changes (not depicted).

The data obtained with transient K^+ currents of rabbit CB chemoreceptor cells allow us to conclude that many of the modulatory effects of DPPX on Kv4 currents described in the heterologous expression system are also relevant for native currents. However, it must be taken into account that these effects are muffled because the transient K^+ current component does not reflect a homogeneous channel population (Sanchez et al., 2002; López-López et al., 2003; Kääb et al., 2005), and because siRNA against DPPX does not produce a complete knockout of DPPX subunit expression. In spite of these limitations, we can extract relevant and unambiguous conclusions from the data obtained from siRNA DPPX–transfected cells regarding the role of DPPX subunit in rabbit CB chemoreceptor cells: (a) DPPX has a chaperone role on Kv4 currents, as in the presence of siRNA DPPX there is a significant decrease in the current density of the transient component; (b) DPPX accelerates the time course of inactivation of the channels, as DPPX down-regulation decreases the proportion of the fast component of the current; (c) DPPX shifts the voltage dependence of activation to more depolarized potentials, an effect opposed to what is described for Kv4.2 and Kv4.3 but previously found for Kv4.1 channels (Jerng et al., 2004b), which we know are expressed in chemoreceptor cells (Sanchez et al., 2002); and (d) DPPX contributes to TEA sensitivity of transient K^+ current, as siRNA DPPX–transfected cells exhibited a significant decrease of their TEA sensitivity. With regards to this latter observation, it is interesting to point out that the change in TEA sensitivity was not observed along the whole range of TEA concentrations, but only for the high micromolar–low millimolar ones, which in all likelihood represent the Kv4 component of the outward K^+ current (component B2 in Fig. 1). We have previously described that the component blocked by lower TEA concentrations (1–50 µM) represents Kv3.4 channels (Sanchez et al., 2002; Kääb et al., 2005), and this component is not modified by siRNA DPPX, but is reduced by down-regulation of Kv3.4 channels (as under chronic hypoxia stimulation (Kääb et al., 2005), and selectively abolished with transfection of siRNA against rabbit Kv3.4 (unpublished data). On the other hand, at high TEA concentrations, the fraction of the current blocked is a noninactivating one, that we have evidences indicating that is carried by members of the Kv1 family of channels (Perez-Garcia et al., 2000). As the experiments of single cell electroporation of CB chemoreceptor cells are technically demanding, we could not perform a complete TEA dose–response curve in all the cells studied (as the one shown in Fig. 1) so we did not have enough data points to adjust TEA inhibition to a multiple binding site model. However, even with the simple fit to one binding site we found more than a threefold decrease of TEA sensitivity upon DPPX down-regulation, from 171.1 ± 11.4 µM in control to 540 ± 40.8 µM in siRNA DPPX–transfected cells (Fig. 9). Nevertheless, differences in the molecular composition of native Kv4 heterocomplexes could certainly explain differences in TEA sensitivity (both in terms of affinity and magnitude of block) between native and heterologous

expression systems. Altogether, this set of data indicates that the effect of siRNA DPPX is very selective on Kv4 currents and that DPPX association contributes to the atypical pharmacological profile of Kv4 currents in rabbit CB chemoreceptor cells.

We thank Esperanza Alonso for excellent technical assistance.

This work was supported by Ministerio de Sanidad y Consumo, Instituto de Salud Carlos III grants R006/009 (Red Heracles) and PI041044 (J.R. López-López), Ministerio de Educación y Ciencia grant BFU2004-05551 (M.T. Pérez-Garcia) and BFU2007-61524 (J.R. López-López), and Junta de Castilla y León grant VA011C05.

Lawrence G. Palmer served as editor.

Submitted: 23 October 2007
Accepted: 18 March 2008

REFERENCES

An, W.F., M.R. Bowlby, M. Betty, J. Cao, H.P. Ling, G. Mendoza, J.W. Hinson, K.I. Mattsson, B.W. Strassle, J.S. Trimmer, and K.J. Rhodes. 2000. Modulation of A-type potassium channels by a family of calcium sensors. *Nature.* 403:553–556.

Bähring, R., L.M. Boland, A. Varghese, M. Gebauer, and O. Pongs. 2001. Kinetic analysis of open- and closed-state inactivation transitions in human Kv4.2 A-type potassium channels. *J. Physiol.* 535:65–81.

Baldwin, T.J., M.L. Tsaur, G.A. Lopez, Y.N. Jan, and L.Y. Jan. 1991. Characterization of a mammalian cDNA for an inactivating voltage-sensitive K^+ channel. *Neuron.* 7:471–483.

Barry, D.M., H. Xu, R.B. Schuessler, and J.M. Nerbonne. 1998. Functional knockout of the transient outward current, long-QT syndrome, and cardiac remodeling in mice expressing a dominant-negative Kv4 α subunit. *Circ. Res.* 83:560–567.

Beck, E.J., and M. Covarrubias. 2001. Kv4 channels exhibit modulation of closed-state inactivation in inside-out patches. *Biophys. J.* 81:867–883.

Chabala, L.D., N. Bakry, and M. Covarrubias. 1993. Low molecular weight poly(A)+ mRNA species encode factors that modulate gating of a non-Shaker A-type K^+ channel. *J. Gen. Physiol.* 102:713–728.

Jerng, H.H., and M. Covarrubias. 1997. K^+ channel inactivation mediated by the concerted action of the cytoplasmic N- and C-terminal domains. *Biophys. J.* 72:163–174.

Jerng, H.H., M. Shahidullah, and M. Covarrubias. 1999. Inactivation gating of Kv4 potassium channels: molecular interactions involving the inner vestibule of the pore. *J. Gen. Physiol.* 113:641–660.

Jerng, H.H., P.J. Pfaffinger, and M. Covarrubias. 2004a. Molecular physiology and modulation of somatodendritic A-type potassium channels. *Mol. Cell. Neurosci.* 27:343–369.

Jerng, H.H., Y. Qian, and P.J. Pfaffinger. 2004b. Modulation of Kv4.2 channel expression and gating by dipeptidyl peptidase 10 (DPP10). *Biophys. J.* 87:2380–2396.

Jerng, H.H., K. Kunjilwar, and P.J. Pfaffinger. 2005. Multiprotein assembly of Kv4.2, KChIP3 and DPP10 produces ternary channel complexes with ISA-like properties. *J. Physiol.* 568:767–788.

Johns, D.C., H.B. Nuss, and E. Marban. 1997. Suppression of neuronal and cardiac transient outward currents by viral gene transfer of dominant-negative Kv4.2 constructs. *J. Biol. Chem.* 272:31598–31603.

Kääb, S., E. Miguel-Velado, J.R. López-López, and M.T. Perez-Garcia. 2005. Down regulation of kv3.4 channels by chronic hypoxia increases acute oxygen sensitivity in rabbit carotid body. *J Physiol.* 566:395–408.

Liu, L.Y., G.E. Hoffman, X.W. Fei, Z. Li, Z.H. Zhang, and Y.A. Mei. 2007. Delayed rectifier outward K^+ current mediates the migration of rat cerebellar granule cells stimulated by melatonin. *J. Neurochem.* 102:333–344.

Livak, K.J., and T.D. Schmittgen. 2001. Analysis of relative gene expression data using real-time quantitative PCR and the $2(-\Delta\Delta C(T))$ method. *Methods.* 25:402–408.

López-López, J.R., D.A. De Luis, and C. Gonzalez. 1993. Properties of a transient K^+ current in chemoreceptor cells of rabbit carotid body. *J. Physiol.* 460:15–32.

López-López, J.R., C. Gonzalez, and M.T. Pérez-García. 1997. Properties of ionic currents from isolated adult rat carotid body chemoreceptor cells: effect of hypoxia. *J. Physiol.* 499:429–441.

López-López, J.R., M.T. Perez-Garcia, G. Sanz-Alfayate, A. Obeso, and C. Gonzalez. 2003. Functional identification of Kvα subunits contributing to the O_2-sensitive K^+ current in rabbit carotid body chemoreceptor cells. *Adv. Exp. Med. Biol.* 536:33–39.

Malin, S.A., and J.M. Nerbonne. 2001. Molecular heterogeneity of the voltage-gated fast transient outward K^+ current, I(Af), in mammalian neurons. *J. Neurosci.* 21:8004–8014.

Martina, M., J.H. Schultz, H. Ehmke, H. Monyer, and P. Jonas. 1998. Functional and molecular differences between voltage-gated K^+ channels of fast-spiking interneurons and pyramidal neurons of rat hippocampus. *J. Neurosci.* 18:8111–8125.

Nadal, M.S., A. Ozaita, Y. Amarillo, E. Vega-Saenz de Miera, Y. Ma, W. Mo, E.M. Goldberg, Y. Misumi, Y. Ikehara, T.A. Neubert, and B. Rudy. 2003. The CD26-related dipeptidyl aminopeptidase-like protein DPPX is a critical component of neuronal A-type K^+ channels. *Neuron.* 37:449–461.

Nadal, M.S., Y. Amarillo, E. Vega-Saenz de Miera, and B. Rudy. 2006. Differential characterization of three alternative spliced isoforms of DPPX. *Brain Res.* 1094:1–12.

Nerbonne, J.M. 2000. Molecular basis of functional voltage-gated K^+ channel diversity in the mammalian myocardium. *J. Physiol.* 525:285–298.

Nerbonne, J.M., and R.S. Kass. 2005. Molecular physiology of cardiac repolarization. *Physiol. Rev.* 85:1205–1253.

Pak, M.D., K. Baker, M. Covarrubias, A. Butler, A. Ratcliffe, and L. Salkoff. 1991. mShal, a subfamily of A-type K^+ channel cloned from mammalian brain. *Proc. Natl. Acad. Sci. USA.* 88:4386–4390.

Patel, S.P., and D.L. Campbell. 2005. Transient outward potassium current, 'Ito', phenotypes in the mammalian left ventricle: underlying molecular, cellular and biophysical mechanisms. *J. Physiol.* 569:7–39.

Pérez-García, M.T., A. Obeso, J.R. López-López, B. Herreros, and C. Gonzalez. 1992. Characterization of cultured chemoreceptor cells dissociated from adult rabbit carotid body. *Am. J. Physiol.* 263:C1152–C1159.

Perez-Garcia, M.T., J.R. López-López, A.M. Riesco, U.C. Hoppe, E. Marban, C. Gonzalez, and D.C. Johns. 2000. Viral gene transfer of dominant-negative Kv4 construct suppresses an O_2-sensitive K^+ current in chemoreceptor cells. *J. Neurosci.* 20:5689–5695.

Perez-Garcia, M.T., O. Colinas, E. Miguel-Velado, A. Moreno-Dominguez, and J.R. López-López. 2004. Characterization of the Kv channels of mouse carotid body chemoreceptor cells and their role in oxygen sensing. *J. Physiol.* 557:457–471.

Radicke, S., D. Cotella, E.M. Graf, U. Ravens, and E. Wettwer. 2005a. Expression and function of dipeptidyl-aminopeptidase-like protein 6 as a putative β-subunit of human cardiac transient outward current encoded by Kv4.3. *J. Physiol.* 565:751–756.

Radicke, S., D. Cotella, E.M. Graf, U. Ravens, and E. Wettwer. 2005b. Expression and function of dipeptidyl-aminopeptidase-like protein 6 as a putative β-subunit of human cardiac transient outward current encoded by Kv4.3. *J. Physiol.* 565:751–756.

Rae, J.L., and R.A. Levis. 2002. Single-cell electroporation. *Pflugers Arch.* 443:664–670.

Ren, X., Y. Hayashi, N. Yoshimura, and K. Takimoto. 2005. Transmembrane interaction mediates complex formation between

peptidase homologues and Kv4 channels. *Mol. Cell. Neurosci.* 29:320–332.

Rudy, B., J.H. Hoger, H.A. Lester, and N. Davidson. 1988. At least two mRNA species contribute to the properties of rat brain A-type potassium channels expressed in *Xenopus* oocytes. *Neuron.* 1:649–658.

Sanchez, D., J.R. López-López, M.T. Perez-Garcia, G. Sanz-Alfayate, A. Obeso, M.D. Ganfornina, and C. Gonzalez. 2002. Molecular identification of Kvα subunits that contribute to the oxygen-sensitive K^+ current of chemoreceptor cells of the rabbit carotid body. *J. Physiol.* 542:369–382.

Sanguinetti, M.C., J.H. Johnson, L.G. Hammerland, P.R. Kelbaugh, R.A. Volkmann, N.A. Saccomano, and A.L. Mueller. 1997. Heteropodatoxins: peptides isolated from spider venom that block Kv4.2 potassium channels. *Mol. Pharmacol.* 51:491–498.

Serodio, P., C. Kentros, and B. Rudy. 1994. Identification of molecular components of A-type channels activating at subthreshold potentials. *J. Neurophysiol.* 72:1516–1529.

Song, W.J., T. Tkatch, G. Baranauskas, N. Ichinohe, S.T. Kitai, and D.J. Surmeier. 1998. Somatodendritic depolarization-activated potassium currents in rat neostriatal cholinergic interneurons are predominantly of the A type and attributable to coexpression of Kv4.2 and Kv4.1 subunits. *J. Neurosci.* 18:3124–3137.

Takimoto, K., E.K. Yang, and L. Conforti. 2002. Palmitoylation of KChIP splicing variants is required for efficient cell surface expression of Kv4.3 channels. *J. Biol. Chem.* 277:26904–26911.

Tkatch, T., G. Baranauskas, and D.J. Surmeier. 2000. Kv4.2 mRNA abundance and A-type K^+ current amplitude are linearly related in basal ganglia and basal forebrain neurons. *J. Neurosci.* 20:579–588.

Wada, K., N. Yokotani, C. Hunter, K. Doi, R.J. Wenthold, and S. Shimasaki. 1992. Differential expression of two distinct forms of mRNA encoding members of a dipeptidyl aminopeptidase family. *Proc. Natl. Acad. Sci. USA.* 89:197–201.

Xu, H., D.M. Barry, H. Li, S. Brunet, W. Guo, and J.M. Nerbonne. 1999. Attenuation of the slow component of delayed rectification, action potential prolongation, and triggered activity in mice expressing a dominant-negative Kv2α subunit. *Circ. Res.* 85:623–633.

Zhang, M., M. Jiang, and G.N. Tseng. 2001. minK-related peptide 1 associates with Kv4.2 and modulates its gating function: potential role as β subunit of cardiac transient outward channel? *Circ. Res.* 88:1012–1019.